TU Delft
Biomedical Engineering
Biomechatronics track

Master Thesis

Effect of series versus parallel electrical configuration on self-sensing in a structure of twisted and coiled polymer muscles.

M. Röling

27-11-2017

Chair: Dr. Ir. H. Vallery
Mentor: Ir. J.O. Van Der Weijde
Contact: m.roling@student.tudelft.nl

Effect of series versus parallel electrical configuration on self-sensing in a structure of twisted and coiled polymer muscles.

Master Thesis

At the TU Delft, faculty of Biomedical Engineering, Biomechatronics track.

M.Röling 4004000 mroling@student.tudelft.nl

Chair Dr.Ir.H.Vallery Mentor Ir.J.O.VanDerWeijde

***Abstract*—The Twisted and Coiled Polymer Muscle (TCPM) is a new, light weight compliant actuator that is easy and inexpensive to produce. As a result there is a growing body of research, with the goal of implementation of the TCPM. Our research combines two existing fields: 1. Self-sensing, eliminating the need for an external force and displacement sensor. 2. Structures of multiple TCPMs. This research compares the effect of a series versus parallel electrical configuration on self-sensing in Joule heated TCPMs. Experiments show that both series and parallel connection are fit for self-sensing. Relative errors in series configuration are 6.7 % 6.9 % and 5.1 % for respectively strain, temperature and force. Relative errors in parallel configuration are 8.3 % 10.4 % and 7.8 %. These data show series configuration performs better on self-sensing accuracy. This is due to the 2-3 dB difference in signal to noise ratio, in favour of series. In addition good repeatability was found in the mechanical behaviour of the TCPMs, with a variance in the spring constant that is smaller than 10 % for all cases. This research therefore demonstrates good repeatability as well as accurate self-sensing in a structure in favour of a series electrical configuration.**

I. Introduction

Research to compliant actuators is gaining momentum. This is due to the safety of compliant actuators when interacting with humans, robots and uncertain environments. Within the field of compliant actuators there is an increasing body of research to artificial muscles.

The artificial muscle is defined as: 'materials that can reversibly contract, expand or rotate within one component due to an external stimulus' [1]. Examples of materials are: piezoelectric materials, magnetostrictive materials, dioelectric elastomers, shape memory metals, carbon nanotubes and conductive polymers, among others [2]. The increase to research in the field of artificial muscles can be explained by the promising specifications, such as: compactness, weight and costs. Haines et al. [3] have discovered that nylon threads can be used as an artificial muscle. In general the nylon threads are twisted and coiled into a helix structure. Resulting from the created structure, the twisted and coiled polymer muscle (TCPM) will contract, expand or rotate as a result of temperature change. The results are outstanding compared to other artificial muscles, in terms of work density, power density and stroke. In addition, the manufacturing is easy and inexpensive.

The effect of these positive specifications, is that other research groups have joined the research community for TCPMs. There is a clear agreement on the working principle [4, 5, 6, 7, 8]. There are two main reactions nylon has to temperature increase that are sequential. 1. Increase in temperature above the glass-transition temperature results in a decrease the intra-molecular space in the amorphous regions of the nylon. As a result the nylon thread contracts in axial direction, around 4 % [3]. This phenomenon is called the negative thermal expansion. 2. When the latter process is satisfied, the molecular

structure will expand in diameter [5].

Based on these main working principles of the TCPM, different decisions affect the final mechanical behaviour.

As a first, the heat source to activate the TCPM should be considered. Generally speaking convection (such as, warm air), radiation and conduction (such as, via a resistive wire) are the main options. This decision will affect the heating and cooling time of the TCPM and might affect the uniformity of the temperature.

Secondly the construction type chosen, will affect the force and strain of the TCPM. Main choices in TCPM construction to be differentiated are: auto-coiled (high load capacity) versus mandrel coiled (high stroke). The latter can be heterochiral (expanding) or homochiral (contracting). The number of twisted strings intertwined, named as mono-ply, two-ply and multi-ply, should be considered. A well referenced example is the TCPM of Haines et al. [3]; by twisting and coiling, the axial contraction is increased up to 34% of the original length (here an auto-coiled, homochiral single-ply TCPM was created).

And thirdly, the use of multiple TCPMs in a structure. Kianzad et al. [9] have reported on a structure of multiple TCPMs. They used a pennate structure including 16 auto-coiled TCPMs and focussed on the effect of recruitment on the stiffness. They found a factor 9 stiffness variation in their experiment, depending on the passive or active state of the TCPMs. A structure of multiple TCPMs can have many benefits, including: increase the degrees of freedom [10], tune and increase stiffness [9], force or strain.

Although researchers agree on the working principle, the characteristic findings differ among research parties. This is most likely due to differences in the many choices, not only in actuation and structure, but also in; type of nylon used, production protocol (twists, coils and annealing), training and testing. This highlights the importance to note all the above decisions and corresponding characteristics.

When using a conductive wire (wrapped around the nylon thread) as the heat source, added value can be gained from the measure of electric impedance. It is known that the mechanical en electrical properties of the TCPM change with its state. It has been proven that the electrical properties, resistance and inductance, can be mapped to the mechanical properties[11, 12, 13, 14, 15]. The mechanical state can therefore be determined by measuring the electrical properties. Since the electrical resistance and inductance can be measured with the input signal, the term self-sensing is used.

In TCPMs self-sensing has first been proven by Van der Weijde et al. [11], who validated their model to have less than 1 % relative RMSE for displacement and temperature sensing and less then 10 % relative error for force sensing. The work of Van Der Weijde et al. [11] as well as the research of Kim et al. [13] and our own research, are based on the general principles of 1. electrical coil inductance and 2. electrical resistance. These are dependant on deflection and temperature [12, 16]. Self-sensing is a major improvement for all applications where TCPMs need to be controlled, since it eliminates the need for other (often larger and heavier) external sensors. Other sensors are used for feedback in Joule heated TCPMs, such as in the research of Arakawa et al. [17]. They report positive results from a feedback controller for a Joule heated TCPM. Their work would be more easily implemented for self-sensing than an external laser displacement sensor.

This research will combine the field of self-sensing with the field of using multiple TCPMs in a structure. The goal of this research is to compare a series versus parallel electrical connection, for the self-sensing of a structure of multiple TCPMs. The TCPMs used are; homochiral, mandrel coiled, single-ply and activated via Joule heating.

In the first part of the study considers the mechanical behaviour of one TCPM and its repeatability, as well as the repeatability of the behaviour between TCPMs. A total of ten TCPMs are tested in a dynamic strain experiment to determine the repeatability of the mechanical behaviour between TCPMs. One TCPM is tested for 10 times to determine the repeatability within one TCPM. The spring constant is used as mechanical property to determine the mechanical behaviour and variations in spring constant is used to determine the repeatability.

The second part of the study elaborates on the

self-sensing experiment in a structure of two TCPMs, where the goal is to differentiate between a series and parallel electrical configuration. A model introduces the mapping functions from electrical to mechanical properties. A structure of two TCPMs, that are mechanically fixed in parallel, is tested at three different actuation temperatures. Double datasets are generated for both series and parallel measurements. One dataset is used to find the mapping between the mechanical and electrical values, the second dataset is used to evaluate the model-fit.

In this paper the materials and methods are divided into three sections, Section II presents the TCPM production, Section III introduces the self-sensing formula's and series versus parallel model, and Section IV describes the experiments. In the latter section elaborates on both the mechanical repeatability and self-sensing experiment. Results of these experiments are presented in Section V and discussed in Section VI. Section VII draws conclusions from this research.

II. TCPM CONSTRUCTION

This subsection describes the materials used, production and training that result in the TCPMs. These TCPMs are used in the mechanical repeatability and self-sensing experiments.

II.I Materials

This study uses nylon 6.6 (0.6 mm diameter), from Midnight Moon, as well as an iron wire (0.2 mm diameter), from Eurofysica. This resistance has a Positive Temperature Coefficient (PTC). For the production, a set-up is made from a normal drill with a tachometer on one side and a pulley system with a weight on the other. A regular measuring tape is used to measure the lengths of the wires. The mandrel is a hollow stainless steal rod (5 mm diameter, 50 mm length), with special insertions that allow fixation of the wire to the rod. For annealing a *Pol-eko-aparatura type SLW 32 STD* oven is used, with 100 % fan for air circulation.

II.II Production procedure

A manual production protocol is used. There are three general steps in the production. 1. Knot the wires to both ends of the production line. Insert twist in the iron wire and nylon thread of the same length in parallel, under constant load. Twists are inserted by a drill. Twisting is stopped when auto-coiling occurs and the maximum twist density is reached. 2. Wrap the newly created thread around a mandrel, in the same direction as the twisting to create a homochiral TCPM. Connect ends to mandrel and cut from production line. 3. Anneal the materials on the mandrel for one hour to enable the nylon to retain their shape. Then the TCPM is taken off the mandrel.
Due to improved insights, the annealing temperature is changed from 180 °C in repeatability experiments, to 175 °C in self-sensing experiments. For the variance in the TCPMs, it is important that the materials and production are constant. Factors of influence can be found in Appendix A.

II.III Training

To have an optimal repetitive behaviour, many researchers describe the need for training [18, 19, 2, 5, 20, 21, 11]. However, the training methods reported are not consistent.
In a pilot study (see Appendix A) a proper training was found. This training consists of five heating cycles. One heating cycle consists of four steps. 1. Heating the oven to 80 °C. 2. When this temperature is reached, hold the temperature for uniformity of temperature (one minute). 3. Perform strain cycles, strain to 60 % of its original length (at 3 mm/s) for five times. Hold temperature during these strain cycles. 4. Cool down, to 30 °C in five minutes, by external fan.

III. MODEL

This section is divided into three subsections, the first introduces the general equations for inductance (L) and resistance (R). The second part introduces the mapping functions and reasoning. The third part elaborates on the difference between a series and parallel configuration and the effect on self-sensing.

III.I General equations

The general equations that determine electrical resistance and inductance are (1) and (3).

Resistance depends on the original resistance R_0 (in Ω) at a certain temperature (T_0), see (1).

$$R_0 = \rho \frac{l_r}{A_r} \tag{1}$$

The original resistance depends on an electrical resistivity constant (ρ) and two geometrical measures: 1. the length of the resistive wire (l_r in m) and 2. the diameter of the resistive wire (A_r in m^2). The total resistance is given in (2), where the relation between resistance and temperature is taken into account.

$$R = R_0(1 + \zeta(T - T_0)) \tag{2}$$

In (2), ζ is the temperature constant. T is the current temperature and T_0 is the original temperature, both in °C.
The inductance (3) is denoted as L in H.

$$L = \mu_0 \frac{N_l^2}{l_l} \pi r_l^2 \tag{3}$$

In the inductance equation (3), μ_0 is the constant for magnetic permeability of a vacuum, N_l is the number of windings of the helix, l_l is the length along the principal axis of the helix and r_l is the radius of the helix. l_l and r_l are given in m.

III.II Mapping functions

Parts of the equations of the electrical properties (2) (3) are mechanical aspects. These are the basis for the mapping functions that are used to translate the electrical properties into the mechanical state of the TCPM.
The resistance (2) has a positive relation to temperature. The inductance purely depends on the geometry of the structure (3) [13] and is therefore affected by the strain (Δx), this relationship is negative. The force of the TCPM depends on both strain and temperature. The relationship with force and strain depends on the spring-constant of the TCPM and is a positive relationship. The temperature causes the nylon to contract and therefore increase the force.
For large strains that stretch the resistive wire the resistance increases. This is a result of increase in l_r and decrease in A_r. This effect probably occurs after the helical structure of the TCPM has reached its maximal stretch. For high temperatures the diameter of the nylon thread increases. This causes a small change in the geometry of the TCPM, therefore affecting the inductance. This effect is likely to occur after the nylon thread has reached maximal axial contraction. Since both effects only occur for respectively high strains and high temperatures, that are outside the scope of this research, they are not included in the self-sensing formulas.
Resulting from the above reasoning, parametric mapping functions are formulated (4), (5) and (6). These functions translate between electrical state (L R) and mechanical state (Δx T F).
In (4) R is mapped to T, using parameters α and α_0. α quantifies the responsivity of R to a change in T and α_0 is the offset. Where the offset is the resistance at the original temperature.

$$R(T) = \alpha \Delta T + \alpha_0 \quad \leftrightarrow \quad T(R) = \frac{R - \alpha_0}{\alpha} \tag{4}$$

In (5) L is mapped to Δx, using the parameters β and β_0 and the constant x_0. β quantifies the responsivity of L to a change in Δx, x_0 is the original TCPM length and β_0 is the offset. Where the offset is the inductance for the non strained TCPM.

$$L(\Delta x) = \frac{\beta}{\Delta x + x_0} + \beta_0 \leftrightarrow \Delta x(L) = \frac{\beta}{L - \beta_0} - x_0 \tag{5}$$

In (6) Δx and T are mapped to F, using parameters γ_T, γ_x and γ_0. γ_T quantifies the responsivity of F to a change in T, γ_x quantifies the responsivity of F to a change in Δx and γ_0 is the offset.

$$F(\Delta x, T) = \gamma_T T + \gamma_x \Delta x + \gamma_0 \tag{6}$$

By fitting these functions on experimental data, the parameters (α, α_0, β β_0, γ_T, γ_x and γ_0) are estimated.

III.III Parallel versus series

In a structure of multiple TCPMs, a decision on the electrical configuration needs to be taken. Two configurations to consider are series and parallel electrical configurations. The decision affects the input of the mapping functions and therefore the outcome.

The main formulas for the total resistance and inductance of a series and parallel circuit are (7-10). In these equations R_{tot} and L_{tot} stand for the total resistance and inductance of the electrical circuit. The subscripts 1, 2 and n denote the number of elements that are included in the electrical circuit.

$$R_{\text{tot}} = R_1 + R_2 + .. + R_n \tag{7}$$

$$L_{\text{tot}} = L_1 + L_2 + .. + L_n \tag{8}$$

$$R_{\text{tot}} = \frac{R_1 R_2 .. R_n}{R_1 R_2 + R_2 R_3 + R_1 R_3 .. + R_{n-1} R_n} \tag{9}$$

$$L_{\text{tot}} = \frac{L_1 L_2 .. L_n}{L_1 L_2 + L_2 L_3 + L_3 L_1 .. + L_{n-1} L_n} \tag{10}$$

Each electrical circuit is in essence a combination of series and parallel elements. A structure of two TCPMs is used to model the difference of the series and parallel configuration. Appendix F introduces more than two TCPMs and presents proof that the model with two TCPMs gives conclusive results for all electrical configurations. The model is described by (7-10) and the mapping functions. Table I gives example input values. To emulate reality, a measurement error is added to the model, 5 % error on series and 10 % error on parallel configuration. The modelled error is large to show an effect. The error is larger for parallel, since lower values are more difficult to measure and are affected more by noise in the system.

The optimal signal for self-sensing has a large responsivity and a low variance, for optimal precision and accuracy. If s_r is the responsivity and s_v is the variance, the optimal signal is s_r/s_v. This is represented in the Signal to Noise Ratio (SNR), (11) in dB. This SNR is calculated in the model for variance including, only standard deviation and standard deviation plus measurement error.

$$\text{SNR} = 10\log_{10}\frac{s_r}{s_v} \tag{11}$$

From (7) and (8) it can be deduced that, in series the value of R and L, the responsivity to T and Δx, and the variance will all increase with respect to the single TCPM. From (9) and (10) it can be deduced that, in parallel the value of R and L, as well as the responsivity to T and Δx, and the variance will decrease with respect to the single TCPM. Since the responsivity and variance both scale by the same order, the SNR will be similar. Therefore it is suggested that the difference is a result of measurement error.

Table I: Example values as input for the model. These values are roughly based on pilot studies, with an increased σ (50 %) for visual aid.

	μ range	σ	unit
R	5 - 6.5	0.2	Ω
L	4 - 5	0.05	μH

Table II: Model output: total values of the series and parallel configurations for a structure of two TCPMs. The SNR is calculated excluding (SNRn) and including (SNRe) the measurement error.

Series	μ range	σ	SNRn	SNRe
R	10 - 13 Ω	0.28 Ω	8.5 dB	8.0 dB
L	8 - 10 μH	0.07 μH	5.5 dB	5.1 dB
Parallel	μ range	σ	SNRn	SNRe
R	2.4 - 3.25 Ω	0.07 Ω	8.5 dB	7.6 dB
L	2 - 2.5 μH	0.02 μH	5.5 dB	4.7 dB

The above reasoning is supported by the output of the model, see Table II. Figure 1 visualizes the effect of series and parallel on the self-sensing formulas. The top trends of both graphs visualize the series configuration and the lower trends visualize the parallel configuration. Every trend is built up by three different colors: 1. blue, which represents the mean. 2. red, which represents the standard deviation. 3. yellow, which represents the measurement error. The slope represents the responsivity and the width of the trend represents the variance. It shows that series configuration has a higher slope than parallel configuration and that it has a higher standard deviation. The total mean and standard deviation are calculated. The error is plotted as a variance over the mean. This moves the standard deviation further apart, decreasing the precision of the measurement.

It can be concluded that in theory series and parallel will perform similar for self-sensing. Taking into account measurement error, series is less affected than parallel, since it has higher measurement values. Therefore it is predicted by the model that the series configuration performs better during the experiment.

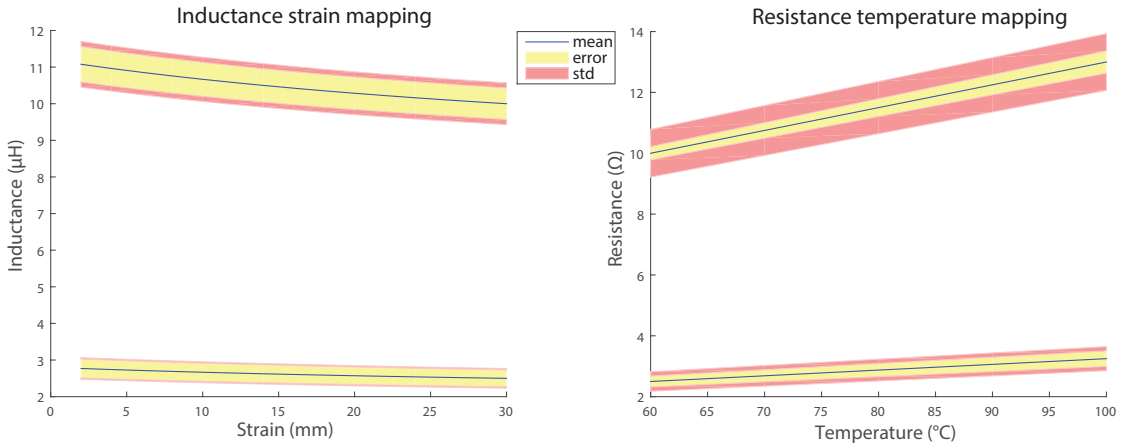

Figure 1: These graphs show modelled mapping lines for inductance to strain and resistance to temperature, each graph shows two lines. Top represents series, bottom represents parallel. These lines consist of a blue mean, a red standard deviation and a yellow measurement error (10 % for parallel and 5 % for series).

Direct versus Indirect self-sensing

In a structure of multiple TCPMs, two distinct ways of self-sensing can be differentiated. The first is direct self-sensing, measuring the structure as a whole and estimating the mapping parameters from here. The second is indirect self-sensing, measuring each TCPM on its own and estimating the mapping parameters for each component.
In indirect self-sensing there are two possibilities for estimation the structure: 1. using the estimated parameters of the single TCPMs to estimate the total parameters of the structure. Then using the total measured R and L to estimate the state of the structure. 2. using the measured R and L of the structure to estimate the R and L of each component. Then use the individual mapping functions to estimate the state of each TCPM. Combine this information to estimate the state of the structure.
Direct self-sensing has the advantage that only the system as a whole is measured. As a result information on each individual TCPM, their mechanical connection and their interaction is implicitly included in the parameters.
Indirect self-sensing excludes the need to measure the structure as a whole. It is therefore possible to make adjustments to the structure without the need of new characterization of the structures parameters. The down side is that information on the structure needs to be explicitly included in a model and/or the mapping functions. This does require a more detailed information of the mechanical structure and neighbouring effects such as: mutual inductance and heat transfer.
This research is limited to direct self-sensing. In addition, a pilot on direct versus indirect self-sensing and neighbouring effects is included in Appendix G.

IV. Experiment

This subsection explains the experimental design, including materials, data processing and data analysis for both experiments.

IV.I Materials

The TCPMs in this experiments are produced as in Section II. The *Zwick/Roell* universal tensile machine (UTM) with heat chamber is used to execute the experiments. The *TestXpert II* software is used to control the UTM and save data on time, temperature, strain and force. The accuracy of the temperature sensor is 0.5 °C. The accuracy of the positioning is 2 μm. The accuracy of the load cell (1 kN) is 0.35 % at 0.2 % of its capacity, resulting in an uncertainty of 7 mN.
For the self-sensing experiment the additional electrical data, resistance and inductance, are collected by a Matlab code that controls the LCR6000 measurement device of *Gw.Instek* (referred to as

the LCR). Four *RG178B/U* cables of 1 m length were used for connecting the TCPM (inside the heat chamber) to the LCR (outside the heat chamber). The relative accuracy of the LCR measurement was 0.2 % for series and 0.3 % for parallel.

IV.II Experimental design

This subsection is further divided in two. First the mechanical repeatability experiment will be elaborated, followed by the self-sensing experiment.

IV.II.I Mechanical repeatability: To cover the repeatability within one sample and between samples, one TCPM is tested ten times, four TCPMs are tested twice and ten TCPMs are tested once. The UTM is calibrated and the oven starts to heat to the set temperature of 80 °C. After holding this temperature for one minute, five strain cycles of 60 % strain (from original length of 50 mm) are induced at a velocity of 3 mm/s. Visuals of the experimental set-up and a detailed protocol are given in Appendix B and C respectively.

III.II.I Self-sensing: To cover the self-sensing experiment, two TCPMs, produced simultaneously are used for this experiment.

The experiment protocol starts with the calibration of both UTM and LCR devices. Followed by a measuring sequence.

The measurement sequence starts with ramping to the set temperature. Followed by a straining sequence starts, increasing in steps of 2 mm with a velocity of 3 mm/s. Each strain step of 2 mm is held for 1 s.

This straining sequence is repeated twice during one period of heating in the oven. During the first strain electrical values are measured in series configuration and during the second strain in parallel configuration. The oven is then opened, cooled down and the whole measurement sequence is repeated. This time, during the first strain electrical measurement is done in parallel configuration and during the second strain in series configuration. Visuals of the experimental set-up and a detailed protocol are given in Appendix B and C respectively.

IV.III Data processing

The mechanical repeatability experiment is dynamic. The self-sensing experiment is segmented with dynamic and static parts that alternate. In the latter experiment, only the static parts of the experiment will be used. Therefore, data processing differs between the two experiments.

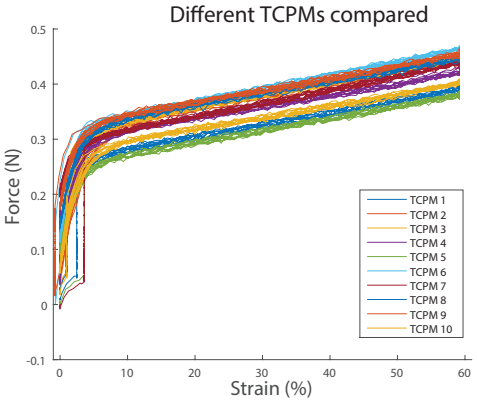

Figure 2: Raw data plot of experiment on 10 TCPMs.

IV.III.I Mechanical repeatability: Cherubini et al. [2] and Moretti et al. [19] both researched the mechanical characterization of the TCPM in a similar strain experiment. They report a pre-load knee at low strains, after which the force increases linear with the strain. They conclude that this pre-load knee is the result of adjacent coils touching each other at the start of the experiment.

The raw data from our experiments show a pre-load knee as well, see Figure 2. After this pre-load knee, the data are linear and without hysteresis. In addition, data from the pilot study in Appendix A supports the theory of touching coils.

To account for the pre-load knee, only the data after 10 % strain are used for further analysis.

IV.III.II Self-sensing: The LCR and UTM sampling rate is 30 Hz and 10 Hz respectively. The UTM datasets show jitter, a deviation from the sample rate. This is compensated for, by interpolating on a linear time scale (10 Hz). For more details on jitter, see Appendix D.

Both electrical and mechanical data are linked and static data are selected based on UTM strain data, by selecting data on the strain plateau's.

For every strain step (Δx), mean and standard deviation are calculated for all measured variables ($R, L, \Delta x, T, F$).

IV.IV Data analysis

The data analysis of mechanical repeatability includes spring constant calculations. The data analysis of the self-sensing experiment includes: spring-constant, Pearson's r, SNR, mapping parameters and model-fit evaluations.

IV.IV.I. Mechanical repeatability: The data can be compared after normalizing the force data on 10 % strain, see (12) where F_n is the normalized force, F is the raw data, F_s is the force on 10 % strain.

$$F_n = F - F_s \tag{12}$$

Thereafter, the spring constant (c in N/m) is calculated, which is used as a measure of mechanical repeatability (see (13), where x is the strain in m).

$$F_n = cx \quad \leftrightarrow \quad c = F_n/x \tag{13}$$

IV.IV.II. Self-sensing: To validate the repeatability of the self-sensing experiment, the spring constant of this static data is calculated, according to (13).

To quantify the relations used by the mapping formulas, Pearson's r (14) is calculated as a measure for correlation. Herein, a and b are measured values. For a is one after an other: Δx, T and F. For a is Δx and T, b is consecutively R and L. For a is F, b is consecutively Δx and T.

$$r = \frac{\sum(a_\sigma - a_\mu)(b_\sigma - b_\mu)}{\sqrt{\sum(a_\sigma - a_\mu)^2 \sum(b_\sigma - b_\mu)^2}} \tag{14}$$

The SNR of the measured signals are calculated. The SNR is defined by (11), where s_r is the change per measured step (for example change in R per 10 °C) and s_v is the standard deviation measured at a step. This standard deviation contains signal variance, noise and measurement error, since it is the measured raw data.

Thereafter, self-sensing parameters are estimated and then validated. The first dataset is used to estimate the parameters of the mapping functions (4) (3) (6), via a regression analysis based on a least square solution.

The mapping function and its estimated parameters are evaluated with the second dataset. The electrical measured values (L R) of the second dataset are input to the mapping functions with the estimated parameters based on the first dataset, to give the estimated mechanical state (Δx_{est} T_{est} F_{est}) as output. These estimates are compared to the measured mechanical state (Δx T F) of the second dataset. This comparison is threefold: Variance Explained (VE) (15) and Root Mean Squared Error (RMSE) (16) in absolute and relative form. In (15)and (16) a is a measured value (Δx T F) and b is the estimated value (Δx_{est} T_{est} F_{est}). The equations sum over all data points (number n) of a.

$$\text{VE} = 1 - \frac{\sum(a_i - b_i)^2}{\sum(a_i - a_\mu)^2} \tag{15}$$

$$\text{RMSE} = \sqrt{\frac{\sum((a_i - b_i)^2)}{n}} \tag{16}$$

Table III: Spring constants of the repeatability experiment, are given in this table.

# TCPMs	# heatings	μ abs.	σ abs.	σ rel.
1	10	5.0 N/m	0.1 N/m	1.0 %
4	2	4.8 N/m	0.2 N/m	4.2 %
10	1	4.7 N/m	0.3 N/m	5.4 %

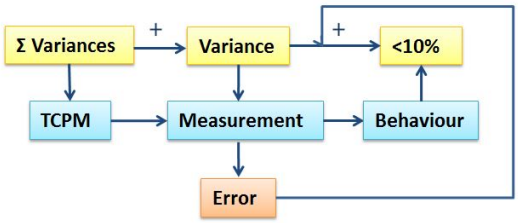

Figure 3: This model shows how variances add to the final repeatability of the TCPMs. Note that the first variance is already the sum of variances of the TCPM production, see Figure 5 in Appendix A.

V. Results

Table III displays the spring constants of the mechanical repeatability experiment. The means of the spring constant are similar, with a combined mean of 4.8 N/m and a standard deviation from this combined mean of 0.2 N/m. Each of the relative deviations are smaller than 6 %, see Table III. These deviations result from multiple variations during production and experiments, see Figure 3.

Table IV presents the spring constants of the self-sensing experiment. The spring constant of the structure of two TCPMs decreases for an increase in temperature. The largest decrease in spring constant, 19.1 N/m decreased to 12.7 N/m,

is found at temperatures 60 °C raising to 70 °C.
Table V shows the signal value ranges and standard deviations, the latter both absolute and relative. The standard deviation value is a measure of variance of the signal. In absolute value the standard deviation is higher in series than in parallel.
Table VI shows the correlation coefficient r for the second parallel dataset. Other datasets give corresponding results. These prove highly significant ($p < 0.01$) correlations for the mapped relationships $R\ T$ ($r > 0.9$), $L\ \Delta x$ ($r > 0.9$), $F\ \Delta x$ ($r > 0.8$) and $F\ T$ ($r > 0.5$).
Table VII displays the results of the SNR for the correlated signals per step, Δx per 2 mm and T per 10 °C. The values of F are lower than those of L and R. SNR values for L and R are above 10 dB, with exception of R in parallel dataset 2. Furthermore, the values of series (S1 and S2) are higher for R and L than the values of parallel (P1 and P2).
Table VIII displays estimated parameters of the first dataset of both series and parallel. These parameters quantify the relationship proven by the correlation coefficient r. The value of the parameter indicates the responsivity of the signal. The values of these parameters for T and Δx (α and β) are higher for series than for parallel configuration.
The self-sensing formula's with parameters from Table VIII and electrical input (L and R) of dataset two, are used to estimate the mechanical state ($\Delta x\ T\ F$) of the TCPM in the second dataset. These estimates with respect to the measured data are represented in Figure 4. The variance in the estimations are smaller in series than in parallel.
Table IX displays the different measures for quantification of model fit: VE, absolute RMSE and relative RMSE. The VE is high, above 90 % in series and above 80 % in parallel. Values are higher for series configuration. RMSE absolute and relative values are small for both series and parallel. These values are smaller for series than parallel: series RMSE are smaller than 7 %, while parallel RMSE are smaller than 11 %.

VI. Discussion

The standard deviation within one TCPM (heated ten times) from the mean is 1.0 % and

Table IV: Spring constants of self-sensing measurement for different temperatures, are given in this table.

T	μ abs.	σ abs.	σ rel.
60 °C	19.1 N/m	0.8 N/m	4.4 %
70 °C	12.7 N/m	0.2 N/m	1.5 %
80 °C	11.7 N/m	0.1 N/m	0.7 %

Table V: The range of measured values and their standard deviations, are given in this table.

	min	max	σ abs.	unit	σ rel.
L_s	16.474	18.408	0.007	μH	0.4%
L_p	3.977	4.473	0.001	μH	0.2%
R_s	11.334	12.240	0.004	Ω	0.4%
R_p	2.851	3.072	0.002	Ω	1%
T	59.0	80.0	0.5	°C	2.4%
Δx	0.00	30.00	0.02	mm	0.1%
F	0.079	0.809	0.008	N	1.1%

Table VI: Pearson's r and its significance for mapped relationships are given in this table. Values are significantly for $p < 0.05$ and correlated for $r > 0.5$. Results for one experiment (parallel dataset 2) are shown, all datasets give similar results as well as uniform conclusions.

	r	p
Δx - L	0.973	0.00
T - R	0.972	0.00
F - Δx	0.825	0.00
F - T	0.533	0.00

Table VII: The SNR dB in responsivity per strain step (2 mm) and temperature step (10 °C) are given in this table, for both parallel (P) and series (S) and both datasets (1,2).

Δx 2 mm	S1	S2	P1	P2
F	7	8	7	8
L	17	18	14	15
T 10 °C	S1	S2	P1	P2
F_max	12	11	11	11
R	12	12	10	9

Table VIII: The parameters estimated on the first dataset, for series and parallel, are given in this table.

parameters	series	parallel	unit
α	0.04	0.01	Ω/°C
α_0	9.01	2.27	Ω
β	224.2	13.8	μH/mm
β_0	13.77	3.32	μH
γ_T	0.01	0.01	N/°C
γ_x	12.55	12.99	N/m
γ_0	-0.30	-0.35	N

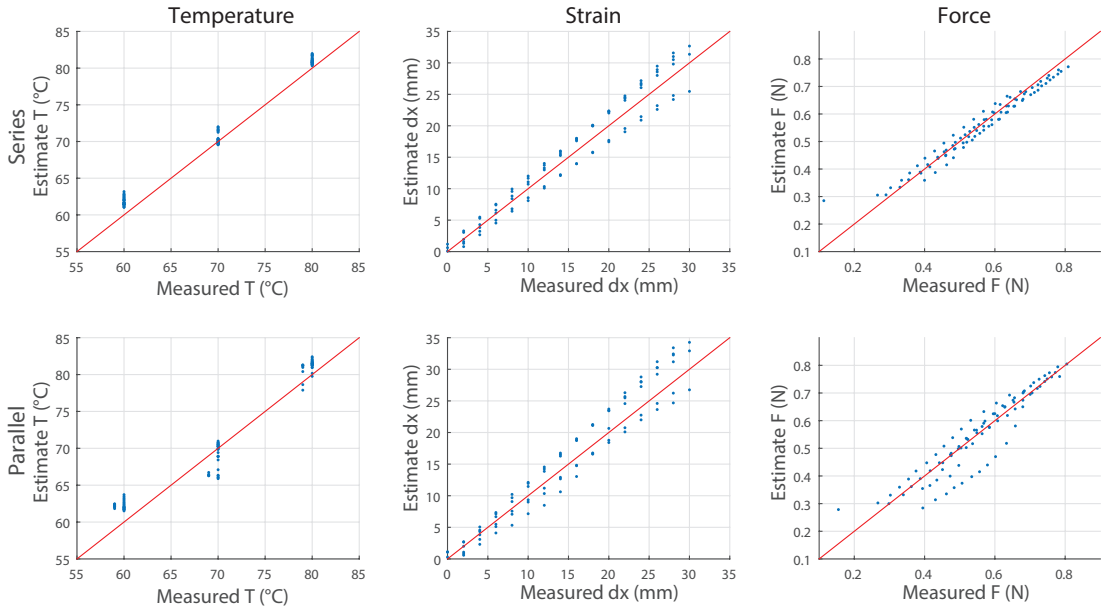

Figure 4: Results of self-sensing in series and parallel configuration are shown on the top and bottom respectively. From left to right are temperature, strain and force. The red bisector line shows a perfect fit, the vertical axis is the estimated value from the self-sensing and the horizontal axis is the measured value.

Table IX: Goodness of fit in VE, absolute RMSE and relative RMSE, are given in this table. Values are shown for series and parallel on estimation of Δx, T and F.

Series	VE	RMSE abs.	RMSE rel.
Δx	94.9%	2.0 mm	6.7%
T	97.1%	1.39 °C	6.9%
F	93.4%	0.04 N	5.1%
Parallel	VE	RMSE abs.	RMSE rel.
Δx	92.2%	2.5 mm	8.3%
T	93.0%	2.17 °C	10.4%
F	84.4%	0.06 N	7.8%

the standard deviation from the mean between ten TCPMs is 5.4 %. It is clear that with the increase in TCPMs tested, the deviation from the mean increases. Taking into account the variance induced during manual production and experiment (see Figure 3), the maximum deviation found is acceptable.

Furthermore, data suggest that with a researched limit of ten heating cycles and five strains each heating, neither the amount of strains nor the amount of heating cycles affect the repeatability.

The spring constant of the self-sensing experiment (shown in Table IV) shows a decrease in stiffness for an increase in temperature. This is in line with the findings of Cherubini et al. [2] and Moretti et al. [19]. Our findings add quantification to the decrease in springs stiffness as well as the mechanical repeatability.

The spring stiffness of the two parallel TCPMs at 80 °C is around double that of the single TCPM. This is expected since the stiffness of two TCPMs are measured, compared to the stiffness of one TCPM. The standard deviation is in the same order as that of the mechanical repeatability experiment. Data suggest an increase in repeatability for an increase in temperature. Additional research is needed to prove this concept. The author suggests an experiment using multiple single TCPMs and perform strain tests on different temperatures for each TCPM. It is suggested by the author that repeatability of mechanical behaviour between TCPMs can be increased by decreasing variables during production.

The model shows a higher variance in the measured R and L for series than for parallel. The absolute standard deviation of the measured signals R and L are higher for series than for parallel. Thus the data supports the model's

prediction.
It is known that mapping functions are based on relation between L Δx, R T and F Δx T. These relations are supported by high and significant Pearson's r values, proving a high correlation.
The model presents a higher responsivity for series than for parallel. The estimated parameter values, that of α and β, quantify the responsivity of R and L. These values are higher for series than for parallel, supporting the model. Further more, γ_x seems to be similar to the spring-constant as expected, the offset values α_0 and β_0 are within the expected range for series as well for parallel.
The SNR, that is dependant on the variance and responsivity, shows a similar trend in the data as in the model. The SNR found in data are higher for series than in for parallel, with a 2-3 dB difference. This difference implies a better model fit for series than for parallel.
The models prediction is a good model fit for both series and parallel, with a favour for series configuration. The model fit on the second dataset is quantified in three ways: VE, absolute RMSE and relative RMSE. VE values are 93-97 % for series and 84-93 % for parallel. Relative RMSE values are below 5.1-6.9 % for series and 7.8-10.4 % for parallel. Therefore the data is supporting the models prediction, both series and parallel have a good model fit. The values (VE, absolute and relative RMSE) are higher for series than for parallel, supporting the models prediction in favour for series configuration. These findings are also in line with data on responsivity, variance and SNR.
Estimation of Δx changes over strain, for a higher strain the RMSE is higher. This phenomenon is also reported by Kim et al. [13], and can be explained by the curved model, where an increase in L is smaller for higher strains.
Estimation of T is the least accurate, it has the highest RMSE. The assumed homogeneous temperature might not have been achieved. This is probably due to the positioning of the temperature sensor, which is next to the heat source.
Estimation of F in relative RMSE is better than the estimation of Δx or T. Since the estimate of F is implicitly dependant on $1/L$ and R it will be affected by the variance in the measured signal and due to the way of mapping these variances have a cancelling effect.
Kim et al. [13] use a third-order formula for the relation of L to Δx. They estimate their parameters via the least squares method, based on a base experiment. The self-sensing accuracy that they report ranges from 5 to 12 % error. These findings are in the same range as the findings in this research.
More interesting is a comparison of our results to those of Van Der Weijde et al. [11], since a similar approach was used. They report very low relative RMSE values (for Δx and T below 1 %) on self-sensing in a single TCPM, where our relative RMSE values for Δx and T are 6.7-10.4 %. The differences between this current research and that of [11] are: 1. the number of TCPMs used in the experiment. Where Van Der Weijde et al. [11] use a single TCPM, our research uses a structure of two TCPMs. 2. the range of temperature used in the measurement, Van Der Weijde et al. [11] used temperatures up to 120 °C, where the limit of this research is set to 80 °C. 3. the mapping functions. Van Der Weijde et al. [11] includes Δx R and T L, which are excluded in this current research. 4. the number of datasets used. This research generates double datasets by including second strain cycles, allowing the use of one dataset for parameter estimation and the other for model fit validation. In contrast, Van Der Weijde et al. [11] uses data from one strain experiment for both estimation of parameters and model-fit validation. The latter of the three differences is most likely the cause for the low relative RMSE reported by Van Der Weijde et al. [11].

Mature sensors reach accuracy errors of 0.5 % or lower. Competing with these sensors means improvement should be made on the self-sensing side. There are three fields of improvement: production, measurement and modelling.
In production the focus will be on eliminating variances induced by production inconsistencies in several ways: 1. optimizing the production protocol, the author suggest a focus on annealing here. An additional approach is to change production from a manual process to an automatic process. 2. controlling the purchased

materials quality. 3. controlling production and storage conditions for: temperature, humidity and UV light, since they are likely to influence the nylons molecular structure.
In the measurement there are two fields of improvement. First, controlling the measurement environment. 1. addition of another sensor for temperature measurement near the TCPMs. This way temperature homogeneity can be proven. 2. change to a load-cell with better specifications for the lower force range measurement. 3. Prevent jitter from occurring during the experiment, see Appendix D. Second, design of the experiment. 1. increase measurement frequencies and use the same frequency for all measurement devices. 2. synchronize data collection from different measurement devices, to enable overlaying mechanical and electrical data. 3. use high frequency alternating series and parallel switching. This way, during the same strain cycle data is collected for both series and parallel configuration, therefore minimizing variances induced by artefacts.
In modelling a more explicit extended error propagation analysis is needed. The author also suggest an model optimization, comparing several linear and non-linear models.

When using the resistive wire (with a positive temperature coefficient) to actuate the TCPM and at the same time estimate the state via self-sensing, parallel and series configuration both have their advantages. A parallel configuration is robust to failure of one of its components, there is no single point of failure. Whereas in series every point is a single point of failure. In series configuration homogeneous temperature can be assumed, since the current is the same for each component. In larger structures it is likely that both parallel and series will be combined. In this case the series to parallel ratio should be well considered, with regard to the SNR.
It might be interesting to take into account the property of the resistance to increase with an increase in temperature. This could imply that in a parallel configuration, the current is higher in lower resistance components and vice versa. Therefore parallel systems might inherently regulate current and therefore control the homogeneity of the systems temperature. It is however questionable whether this results in a stable system, since the increase in resistance is relatively low.
This research focussed on direct mapping, using data of the structure as a whole. The alternative, indirect mapping, is based on the parameters of each of the structures components. The latter is beneficial in a case where one TCPM in a structure changes, since it eliminates the need for a new system calibration. Appendix G presents a pilot study of direct versus indirect self-sensing. This pilot shows a great effect of mutual inductance on the indirect mapping approach. When using indirect mapping, neighbouring effects such as mutual inductance should be included explicitly in the self-sensing's mapping functions, as they are not implicit in the mapping parameters. To understand and model the effect of distance between TCPMs and mutual inductance, a full study is necessary. When using Joule heating to actuate TCPMs in a structure, heat transfer is another neighbouring effect that should be accounted for in the self-sensing's mapping functions. This should in turn be studied.
Another part of future research that the author regards as essential in TCPM research is understanding plastic deformation in the form of tilting. This undesired and ineffective form of deformation is a drawback to the use of these TCPMs, see Appendix E. Understanding this phenomenon is the first step to remove a large obstacle in this research field.

VII. Conclusion

In this paper two studies are performed for the goal of self-sensing in structures of multiple Joule heated TCPMs. In the first study, repeatability is quantified for manually produced TCPMs tested in a dynamic strain experiment. A standard deviation of the spring constant of max 5.4 % is found. Furthermore a decrease in spring constant is found as a result of increasing temperature: 60 to 80 °C causes increase from 11.7 N/m to 19.1 N/m, in a structure of two mechanically parallel TCPMs.
On the main goal of self-sensing in a structure, series and parallel electrical configurations are compared. It can be concluded that both series and parallel configurations perform well. This is

shown by model fit evaluation, VE parallel 84-93 % and series 93-97 %, relative RMSE parallel 8-10 % and series 5-7 %, absolute RMSE for Δx T F smaller in series than in parallel. From this data it can be concluded that series configuration is favoured over parallel configuration. This is the result of a better SNR in series, 3 dB higher than parallel.

This paper has introduced self-sensing in structures of TCPM. Results prove that series is preferred over parallel.

VIII. Acknowledgment

With thanks to:

Ir. J.O. van der Weijde for his input and mentoring on this research. Dr. Ir. H. Vallery for her supervision and support on this research.

Dr. C van der Kamp for this assistance and work on the production line of the TCPMs.

P. van Holst and H. Jansen for the use of and assistance with the UTM of 3ME-PME and their support throughout the process.

IX. Appendix

A. Production and training

This Appendix is divided into a general introduction, production, annealing (heating and cooling) and training, a general conclusion, discussion and future research.

A. I Introduction

In production many decisions effect the performance of the actuals TCPM [5]. The main principle of production contains more or less the same components.

1. Twisting and coiling the nylon string. Decisions that effect the performance of the TCPM are twofold. First, the type of materials used: nylon 6, nylon 6.6, silver coated nylon, and others.
Second, the structure created (as explained in Section I) auto-coiled, mandrel coiled, heterochiral, homochiral, mono-ply or single ply. In case of the need for resistive wire, this is most often included during the twisting and coiling procedure.
2. Annealing is needed to set the mechanical structure, which is required in some structures. The annealing procedure mentioned in many papers [8, 19, 2, 11, 21, 5, 22, 18, 17, 6, 9], used temperatures range from 120-200 °C for a duration ranging between 30-120 minutes. Our use of annealing is optimized by a pilot study that will be the main body of this appendix.
3. Training is needed to gain a repeatable mechanical behaviour. This is reported in many research groups [1, 19, 2, 11, 21, 5, 22, 18, 20]. Some papers report one training cycle [19], others do not specify a number (some cycles, a small number of trainings, ect) [5, 21, 11], whereas Mirvakili et al. [1] use up to 20 cycles. For this research the number of training cycles is explored to find a proper protocol for repeatable mechanical behaviour.
Even when production has a clear protocol, the variance in every production step induces a variance in later mechanical behaviour, see Figure 5. This should be taken into account when interpretating results.
For this work a heterohelixal mandrel coiled TCPM is made from nylon 6 (0.6 mm diameter) inter-twisted with iron wire (0.2 mm diameter), wrapped around a mandrel (6 mm diameter), with annealing and training. This decision allows for a large stroke and self-sensing, to allow for a good analysis of parallel versus series.

A. II Production protocol

The production of TCPMs in this research lab is under fast development. The TCPMs used for this research are produced manually. The steps of production are as follows.

1) Connecting in parallel a nylon and iron wire to a weight of 300 gr and a drill. The 300 gr provide a constant force on the wires.
2) Twist the iron and nylon together until auto-coils appear, at this moment the maximum twist insertion is reached.
3) Coil the new formed wire around a mandrel and fix the ends. Thus creating the final structure.
4) Thermal annealing the structure for 60 minutes at 165 °C, 100 % fan.
5) Cool down the structure for 30 minutes at room temperature.
6) Remove the mandrel.

Effects of variables: During production there are several variables that need to be controlled.

1) Length of the nylon and iron wire at the start.
2) Force exerted during production (in practice, weight connected to the wires).
3) Number of twist inserted by the drill.
4) Number of coils around the mandrel.
5) Diameter of the mandrel.
6) Temperature and time of annealing.
7) Temperature and time of cooling down.

These variables will result in a change in TCPM properties.

1) No direct effect known.
2) A force too high will result in snapping the nylon and iron wire during production. A too low force will influence the total amount of twists inserted for auto-coiling will start earlier.
3) The number of twists will influence the total length of the iron wire in the structure.
4) The number of coils around the mandrel influences the total length of the TCPM also influencing the total force and contraction length. At the same time it influences the resitance and inductance measured.
5) The diameter of the coils will influence the total amount of wire used, therefore the total

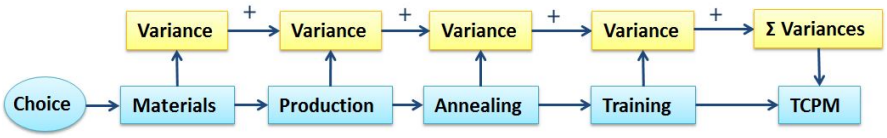

Figure 5: This chart represents the choices during production of the TCPM and their induced variance. The effect of structure is not included explicitly since it is inherent to the production. The variance in materials is due to batch differences and degradation over time. Variance in production is a result of the variables that are not constant. Then with the final variance introduced by training, all variances add up to the total variance of the TCPM.

force and contraction. Also it will effect the inductance and resistance measured.

6) The temperature and time of annealing effects the micro structure of the nylon, changing its ratio of amorphous versus crystalline regions. And thereby influencing the stiffness and flexibility of the nylon and TCPM, as well as the temperature working range and max force.

A. III Annealing

To find the optimal heat treatment for our used nylon 6, different oven temperatures and cooling temperatures are researched in a pilot study.
Annealing and cooling time are kept constant (60 minutes and 30 minutes respectively).

Oven temperature: The first part of this study focussed on the effect of different oven temperatures (160, 170, 180 °C) for annealing and cooling at room temperature (23 °C).
The TCPMs are trained and strained to 60 % at 80 °C. The results are shown in Figure 8. Note that the strain is in mm. The different lengths of strain indicate the different starting lengths of the TCPMs. The pre-load knee theory of Moretti et al. [19], is supported by this data (see Table X). Only the 160 °C annealed TCPM shows a pre-load knee, and it is (in this batch) the only TCPM with touching coils, see Figure 6. There is an increase visible in the maximum force for the increase in annealing temperature. The TCPM annealed at 180 °C did however permanently lengthen, which is considered unwanted behaviour since it degrades the repeatability.

The next day, without training the TCPMs (160 and 170 °C) were tested for increasing actuating temperatures (25, 40, 60, 80, 100, 120 °C) until tilting occurred. These results are shown in Figures 13 and14. It can be suggested that these data indicate that the most effective activation region for TCPM annealed at 160 °C, is between 60 and 80 °C (more than 0.1 N) with a maximum force of around 0.4 N. Whereas the TCPM annealed at 170 °C, the most effective activation region is between 60 and 100 °C (increase per 20 °C around 0.5 N) the maximum force is only around 0.32 N.
Therefore a TCPM annealed at 160 °C and used in the range of 60-80 °C would give the largest controllable force range.

Table X: This table shows the annealing temperature and corresponding resting length of the TCPMs. It also shows if the coils of these TCPMs are touching or not.

annealing °C	length of TCPM mm	coils touch
160	48	yes
170	52	no
180	75	no

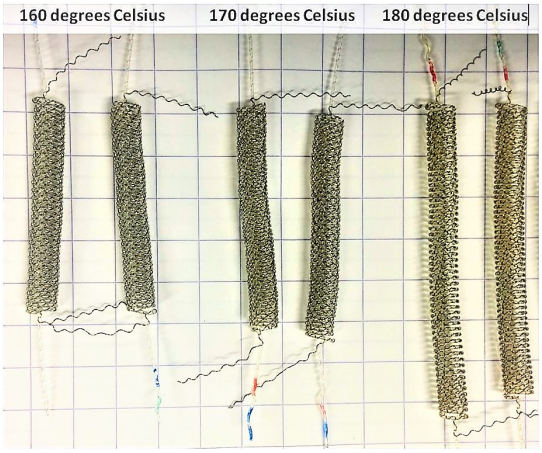

Figure 6: Effect of annealing at different temperatures on the resting length of the TCPMs.

Cooling temperatures: The second part of this research was repeating the experiments as before, however for TCPMs annealed at 165 °C and cooled at 23, 7, -19 °C. The results of training and then testing at 80 °C are shown in Figure 9, the results of testing at different actuation temperatures until tilting occurs are shown in Figures 10, 11 and12. These data indicate that the cooling temperature effects the maximum force (all TCPMs compared at 80 °C), where low temperatures give higher maximum forces. For the lowest temperature (-19 °C) there is a pre-load knee, whereas for other temperatures (7 and 23 °C) there is no pre-load knee. The TCPM lengths in relaxed posture are not different. When looking at different actuation temperatures, the 23 °C cooled TCPM shows a high force increase between 25-40 °C as well as 60-80 °C, with a maximum effectiveness of around 0.02 N and a maximum force of around 0.25 N. The 7 °C shows the most effective range between 60 and 80 °C (an increase in force of around 0.1 N) and a maximum force a little over 0.3 N. The -19 °C data show the most effective range between 40 and 60 °C with an increase of a little over 0.05 N and a maximum force a little over 0.25 N. When looking for the largest controllable force range, the 7 °C cooling temperature is the best.

A. IV Training

After a trial and error method the training of these TCPMs is set to five cycles. One cycle includes heating to 80 °C, stretching to 60 % strain for five times, cooling down to 30 °C in five minutes time.
The raw data output is shown in graph of Figure 7. As is reported by [19] the very first training cycle shows deviation from the rest, however, the first five cycles have a bigger variation than the last five cycles. Supporting the decision to train the TCPMs five times before usage. An additional pilot study regarding the necessity of repeating training after a short period of non-use (one hour), indicates a small effect in re-training, as is visualized in the second graph of Figure 7. Therefore it is considered to be unnecessary to retrain the TCPM after a short time of non-use.
Variables to be controlled during training are the warming time of the heat chamber, temperature of the heat chamber, strain on the TCPM and cooling of time and temperature of the heat chamber. Which includes the speed of the fan and its positioning.

A. V Conclusion

When looking for a TCPM with a high maximum force and a good controllable range of force, annealing with an oven temperature of 170 °C with a cooling temperature of 7 °C is recommended.
It can be concluded that with the current training procedure a repetitive mechanical behaviour can be achieved. After a short period of non-use (one hour) there is no need for re-training.

A. VI Discussion

These experiments are only based on one sample per condition, therefore they are only indications of what to expect. Moreover there seems to be a time factor at play, when comparing the max force of 80 °C on day one and day two of testing. However the data do provide insight into the fact that annealing and cooling affect the behaviour of the TCPM. When training the TCPM the strain force graph and the physical look of the TCPM show if a TCPM is tilting, this happens in some cases and these TCPMs are not applicable for use. This is not reported yet in any literature, but it seems to be a result of internal tension, activation temperature and strain.

A. VII Future research

To truly understand the effects of annealing, there are a couple of future research opportunities. One is to elaborate on this research in a repetitive way, including a bigger temperature range for oven temperature and cooling temperature, as well as a higher resolution. Another option is to investigate the molecular structure of the nylon used and the effect of annealing; a model to predict the outcome of the annealing with respect to mechanical behaviour would be ideal.
Why some TCPMs tilt during training could not be concluded from these experiments. Therefore future research into the tilting phenomenon is needed.

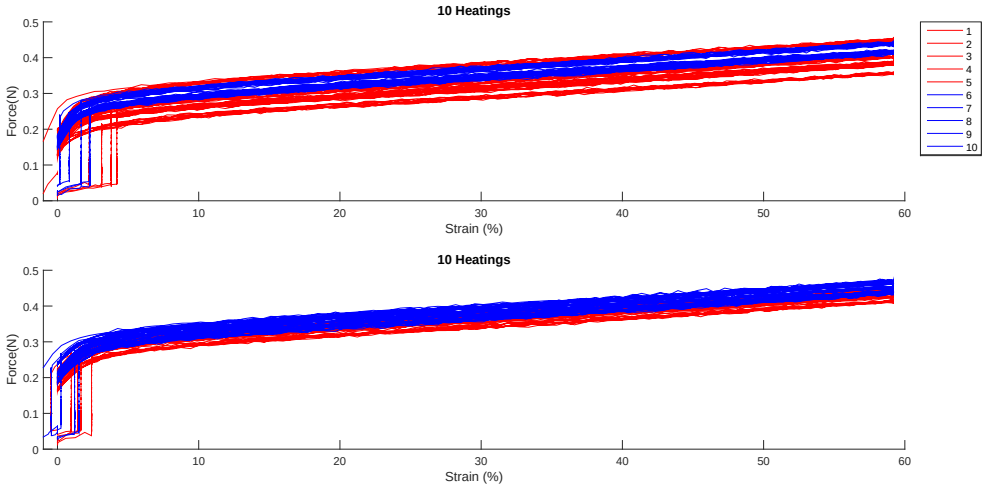

Figure 7: The two graphs in this figure represent each ten heatings of the same TCPM with an one hour period of rest between the heatings. The ten heatings are divided by color into the first five heatings and the second five heatings. It can be observed that the first time of ten heatings the deviation is larger in the first five heatings than in the later five heatings.

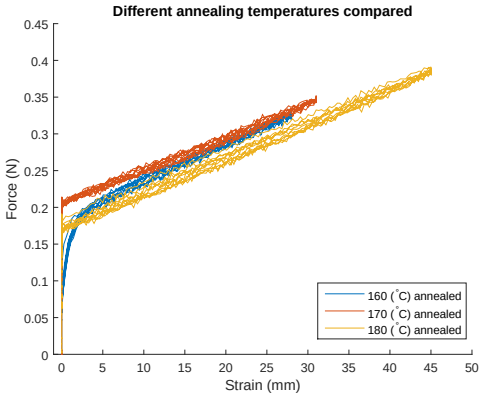

Figure 8: TCPMs annealed at different temperatures, cooled at room temperature. Tested at 80 °C and 60 % strain. Note, start lengths of TCPMs are different for different annealing temperatures.

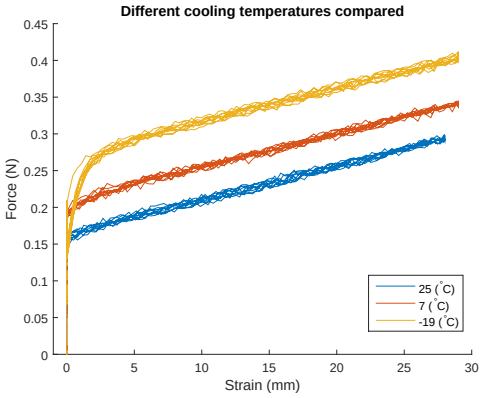

Figure 9: TCPMs annealed at 165 °C, cooled at different temperatures. Tested at 80 °C and 60 % stain.

B. Experimental setup

The two experimental set-ups are described in this section. The first one for the mechanical repeatability experiment, containing the UTM. The second for the self-sensing experiment, containing the UTM and the LCR meter.

B. I Mechanical repeatability

The *Roell/Zwick* universal tensile machine is selected to execute this experiment. The UTM clamps selected for this experiment have a small insert for the nylon thread that can be secured by a small screw. A heat chamber surrounds the clamps and the moving parts of the UTM. The UTM is connected to a PC from where it can be controlled, via the *TestXpertII* software. Figure 15 provides a visual of the experimental set-up, note

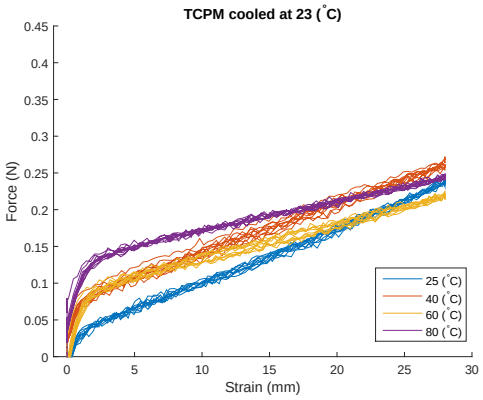

Figure 10: TCPM annealed at 165 °C, cooled 23 °C. Tested at different temperatures and 60 % strain.

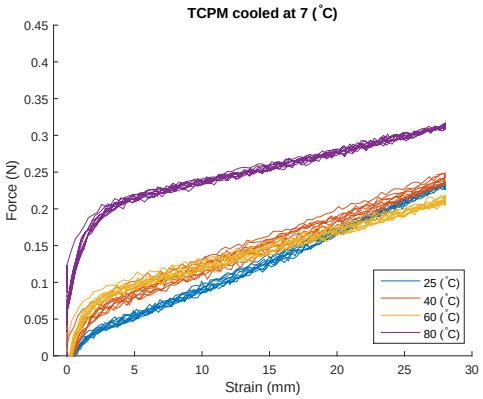

Figure 11: TCPM annealed at 165 °C, cooled 7 °C. Tested at different temperatures and 60 % strain.

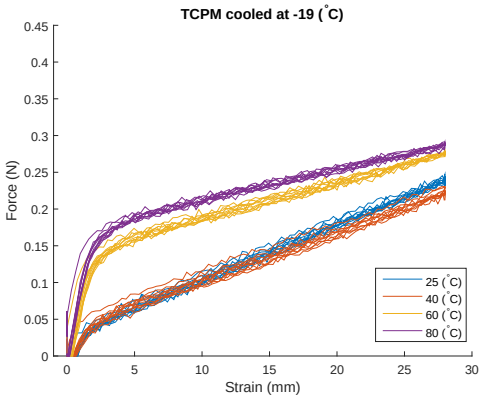

Figure 12: TCPMs annealed at 165 °C, cooled -9 °C. Tested at different temperatures and 60 % strain.

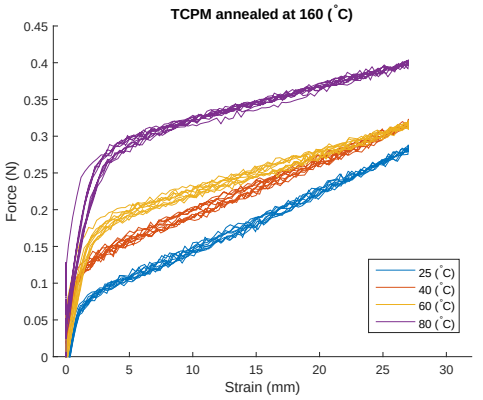

Figure 13: TCPM annealed at 160 °C, cooled at 25 °C. Tested at different temperatures and 60 % strain.

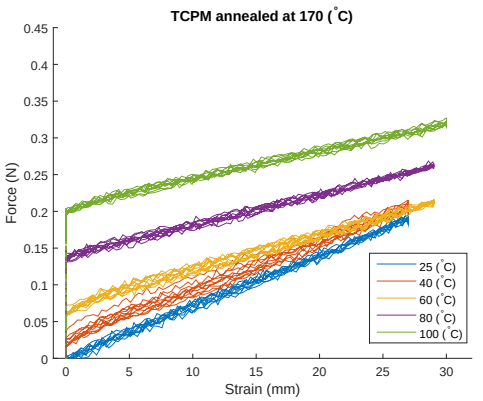

Figure 14: TCPM annealed at 170 °C, cooled at 25 °C. Tested at different temperatures and 60 % strain.

that the LCR shown in the figure is not used in this repeatability experiment.

B. II Self-sensing

For connecting two TCPMs two ceramic terminal blocks are used, they are placed in the centre of the UTM clamps. Another two ceramic terminal blocks are placed on the side of the UTM clamps, they are used to connect the electrical circuit, see Figure 16. To enable the electrical switch between two strain cycles without interfering with the test set-up, a double relay is used. The switch itself is outside the heat chamber, whereas the relay is inside the heat chamber. Four *PRG178B/U* coax cables of 1 m are used to measure inside the heat chamber, while the LCR6000 device is

placed outside the heat chamber on a table. The electrical connection is visualized in Figure 17. A physical electrical circuit (see Figure 18) can be used as an overlay to the photo of the set-up to give insight into the cable connections, see Figure 19. The electrical circuit is carefully designed to have the same wire length and current direction in both parallel and series configuration, therefore reducing the influence on R and L.

Figure 15: This figure shows the experimental set-up of both experiments, although the LCR is not used during repeatability testing. The PC is used to control the UTM (on the right). The heat chamber is the compartment surrounding the clamps of the UTM. For the self-sensing experiment the LCR is used, is connected to the PC on one end and to the TCPM via the clamps on the other end.

C. Experimental protocol

This subsection is divided into two parts, the protocol for the mechanical repeatability experiment and the protocol for the self-sensing experiment.

C. I Mechanical repeatability

The Universile Tensile Machine (UTM) by Zwick/Roell with TestXpert II sofware is used to control the experiment and collect data on time, strain, force and temperature.
The TCPM is tested at 80 °C in this experiment. It is strained to 60 % of its original length of 50 mm.

Protocol: The protocol for the mechanical repeatability experiment is a two phase plan, first the muscle mounting, followed by the measuring.

Figure 16: Clamps of the UTM with four ceramic terminal connectors. The two in the middle are intended for the physical connection of the nylon threads of the TCPM, whereas the two ceramic terminal connectors on the side are intended for the electrical connection of the iron wires.

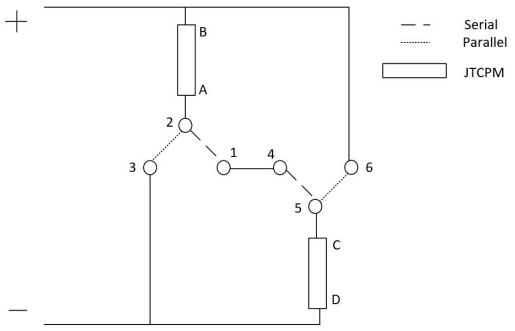

Figure 17: Schematic overview of the electrical circuit. Plus and minus will be provided by the LCR as measurement signal.

Muscle Mounting

1) Suspend the trained TCPM in the top clamp of the UTM.
2) Lower the top clamp, such that the bottom part of the muscle reaches the bottom clamp.
3) Zero force.
4) Attach the bottom clamp.
5) Zero force again and zero displacement.

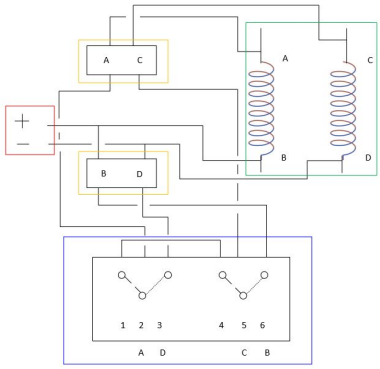

Figure 18: In red is denoted the coax cables from the LCR, that provides the measurement current to the total circuit. In blue is the printed circuit board with a double relay. The relay itself is also connected to the net-power with a switch. For a high current the relay switches to the smallest dots, therefore allowing a parallel connection of the TCPM. For low current the relay switches to its original state of serial connection for the TCPMs. In green the two TCPMs are visualized. Yellow denotes the two ceramic terminal connectors used for the electrical connection.

Measuring
Repeat the following steps for every desired temperature.

1) Ramp to 80 °C.
2) Wait for 60 s.
3) Start straining sequence (3 mm/s to 60 % of original TCPM length, repeat five times).
4) Open heat chamber.
5) Use fan for active cool down.
6) Prepare for next measuring sequence.

C. II Self-sensing

The Universile Tensile Machine (UTM) by *Zwick/Roell* with *TestXpertII* sofware is used to control the experiment and collect data on time, strain, force and temperature. The LCR was used to measure the inductance and resistance. The measurement signal used was set to 100 kHz, parameters for inductance and resistance were set to Ls and Rs respectively.
The TCPM is tested for 80 °C in this experiment. It is strained to 60 % of its original length of 50 mm, with steps of 2 mm.

Protocol: The experiment protocol consists of three parts, calibration, muscle mounting and measuring.
Calibration
The calibration procedure included the following steps:

1) Set LCR settings (100 kHz, Ls-Rs, Fast, Br 115200).
2) Fix measurement cables to the connectors.
3) Trigger open circuit calibration of the LCR.
4) Fix straight copper wire to connectors to short circuit.
5) Trigger short circuit calibration of the LCR.
6) Remove straight copper wire.
7) Measure resistance and inductance of parallel circuit with copper wire.
8) Measure resistance and inductance of serial circuit with copper wire.
9) Measure resistance and inductance of coper wire.

Muscle Mounting
The muscle mounting procedure included the following steps:

1) Suspend the trained TCPM in the top clamp of the UTM.
2) Lower the top clamp, such that the bottom part of the muscle reaches the bottom clamp.
3) Zero force on UTM.
4) Attach the bottom clamp.
5) Attach the conductor the the connectors.
6) Set pre-load to 0.05 N (with automatic displacement to zero).

Measuring
Repeat the following steps for every desired temperature:

1) Set LCR settings (100 kHz, Ls-Rs, Fast, Br 115200).
2) Ramp to the desired temperature.
3) Stay at this temperature for 60 s.
4) Start the LCR measuring sequence.
5) Start the extension and retraction sequence.
6) Switch electrical circuit.
7) After the second strain sequence ends, open heating chamber.
8) Use fan to cool down for five minutes to 30 °C.
9) Prepare for next measuring sequence.

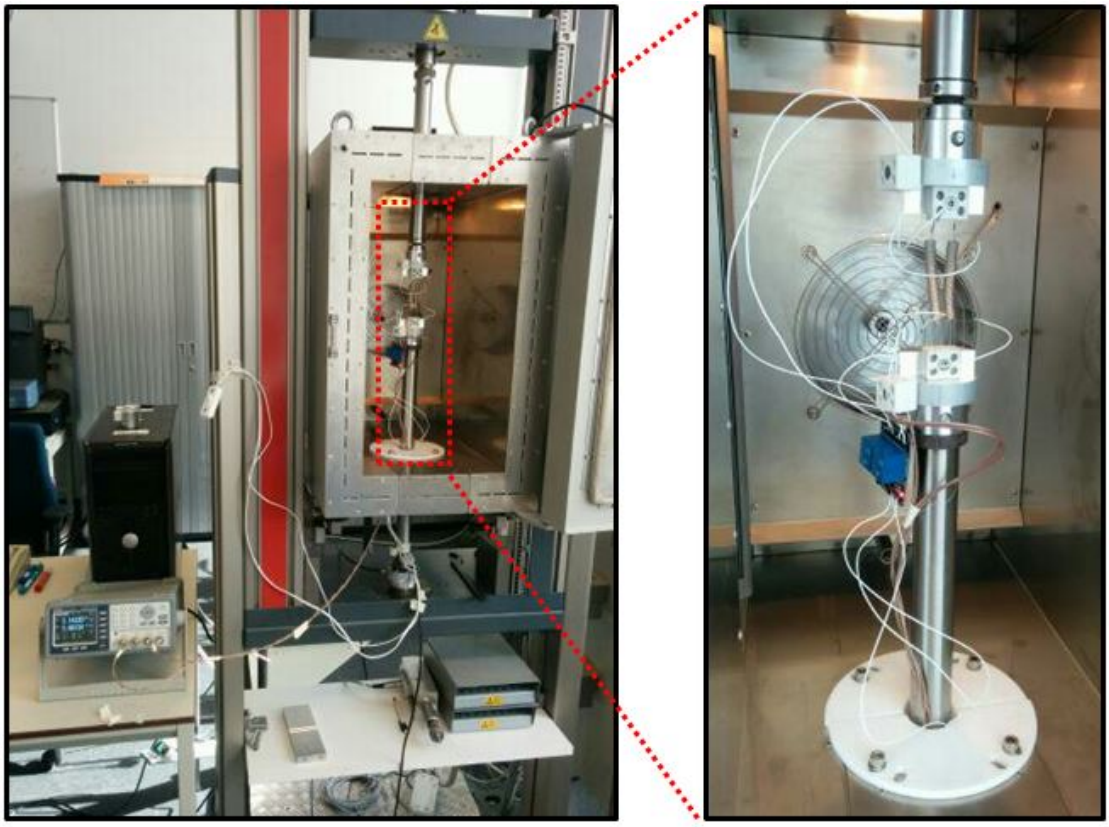

Figure 19: On the left the UTM with LCR and cables are shown, including the switch used to change parallel to series. On the right a close-up of the TCPM connections is shown.

D. Jitter on UTM data

There have been two measurement frequencies during the experiment: first a low frequency, during heating of the oven (first part of linear line in the top Figure 20). Second a higher frequency, during strain test (second part of linear line in the top Figure 20). A deviation of the time vector is visible on the bottom of Figure 20, below the 0.1 s interval line, scatter of higher frequency datapoints is visible. This deviation from a pre-set frequency is known as jitter. Jitter seems to occurs when a change in action of the UTM is required (see location of red dots in Figure 21, force and strain plot). To be more specific, red dots (jitter data) occur when; the experiment is started and stopped, movement is initiated and ended.
Therefore it is assumed, that the high frequency data points are caused by artefact of the UTM software.
Since the time vector is monotone but not linear, it can be corrected by the interpolate function in Matlab using the original frequency of 10 Hz.

E. Plastic deformation

There are two different forms of plastic deformation observed. A linear deformation, that causes the TCPM permanent lengthening, and an angular deformation, that causes a permanent displacement of the coils. The latter is known as tilting. This subsection will elaborate on the occurrence of these two types of plastic deformation, according to two main effectors temperature and strain.

E. I Temperature

There is a limit to the temperature usable for the TCPM. One paper [23] reported on overheating of the TCPM, without any further specifics.

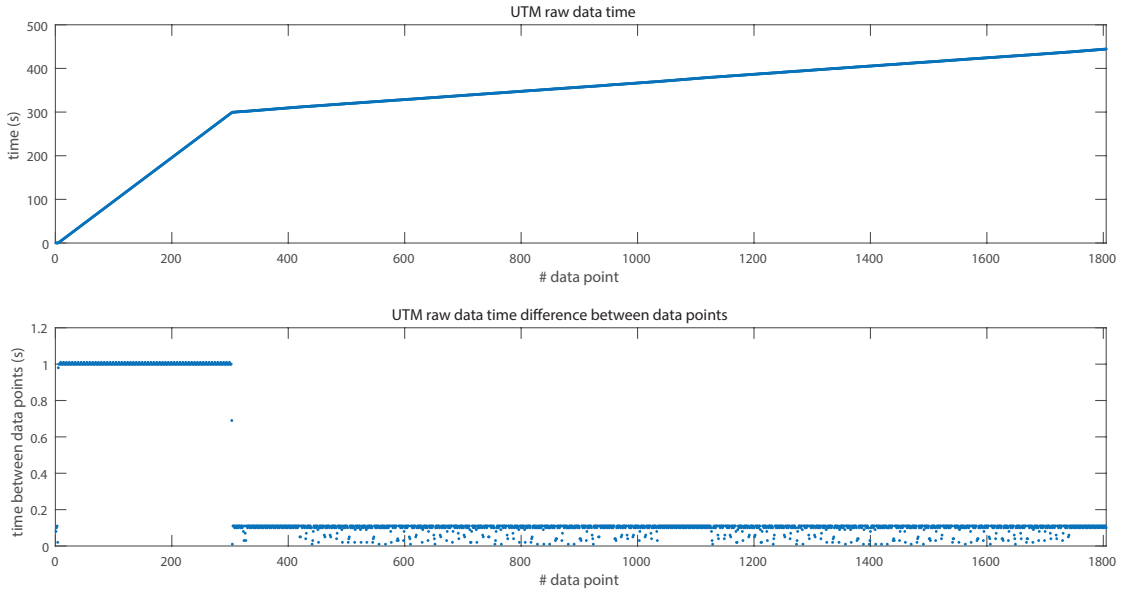

Figure 20: This graph shows the raw data of the UTM on time (top) and time derivative (bottom). An angle is visible in the top graph, representing a shift in the sample frequency. In the bottom graph this angle is represented as a sudden descend. After this descend, scattered data points can be observed below the two mean lines of the sample frequency. This scattered high sample frequency is jitter.

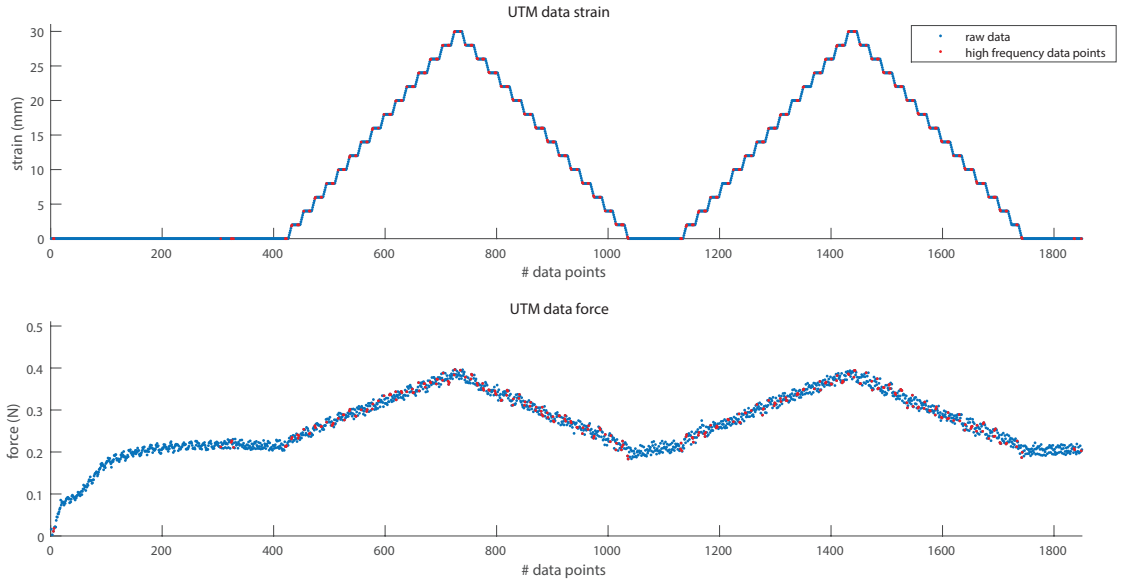

Figure 21: This graph shows the raw data of the UTM on strain and force. The normal frequency data points are blue. The red dots represent the high frequency data points. The top graph (strain) shows that red dots occur around a change, either to initiate or stop the movement of the TCPM, as well as at the start and end of the experiment.

In our pilot study, temperatures higher than 80 °C are prone to tilting, a plastic deformation in an angular fashion (see Figure 23). This deformation causes a large hysteresis in the force strain rela-

tionship, see Figure 22.
During this thesis over 125 TCPMs are produced for testing, of which most are used for repeatability and pilot measures (ten TCPMs are used for self-sensing experiments). For repeatability and understanding the effects of production and training, over 650 experiments are performed. A little under 100 give useful data. All other experiment data are dismissed due to tilting problems. These numbers illustrate the severeness of the problem. The data collection on all TCPMs produced is analysed to look for possible indicator factors for tilting, no significant indicators are found. Time between production and experiment could be a possible factor. Further research into tilting is needed to understand an prevent this phenomenon from occurring.

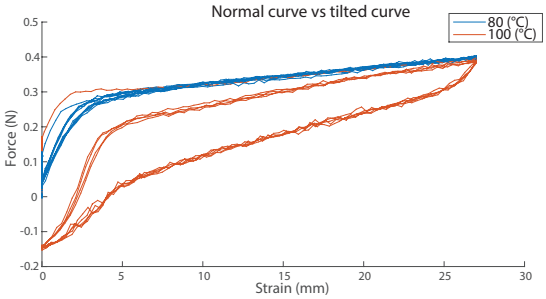

Figure 22: This graph presents the raw data of the experiment on a trained TCPM. It can be seen that at 80 °C the behaviour is normal. At 100 °C the curve is different, a high hysteresis is present and the TCPM is tilted.

E. II Strain

Testing at dictated strains is only reported by Moretti et al. [19] and Cherubini et al. [2], who both strain until 50 % of the original TCPM length. In our experiments a 60 % max is used. A pilot study tested larger dictated strains (up to 150 %), results are shown in Figure 24. At 150 % strain the TCPM suffers linear plastic deformation, permanent increase in resting length. This pilot study indicates that dictated that a strain of up to 100 % does not have a damaging effects on the TCPMs and have little hysteresis.

F. Configurations of electrical circuits

The more elements there are in an electrical circuit, the more different configurations are possible, see Figure 25, for examples of these configurations see Figure 26. The effect of the number of elements in series and parallel is visualized in a model, see Figure 27. Here it is clear that the variance changes with the number of elements in series or parallel: an increase in parallel elements results in a decreasing variance and an increase in series elements results in an increase in variance. An example of two TCPMs is given in figure 28.

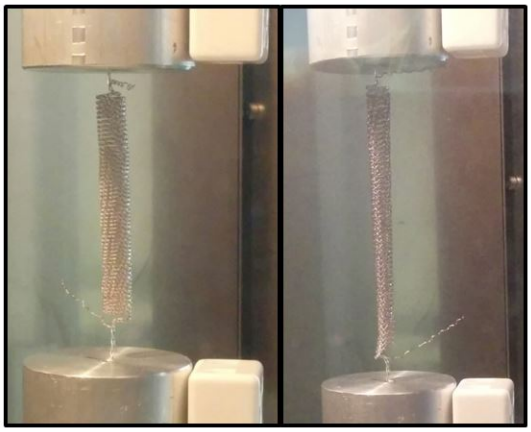

Figure 23: On the left is a TCPM clamped in the UTM not tilted, all coils are parallel to each other and the clamps. On the right is a tilted TCPM, the coils are tilted with respect to the clamp orientation. This effect is more visible at the lower end of the TCPM, due to the tilting orientation and angle of the photo.

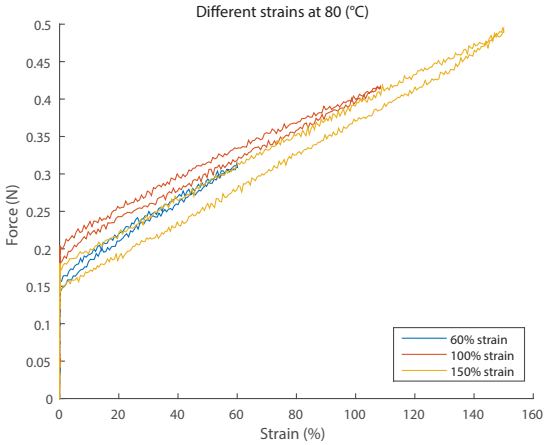

Figure 24: This graph presents data at 60 % 100 % and 150 % strain in different TCPMs. It is visible that the hysteresis is highest at 150 % strain. The maximum force increases for the increase in strain.

For this research the Signal to Noise Ratio (SNR), defined as the responsivity to variance ratio (s_r/s_v) measured in dB is the main indicator for self-sensing accuracy. This SNR is calculated for series and parallel configurations with increasing number of TCPMs (up to $1e6$ elements), the SNR difference is always $<0.01\,\%$. Therefore it can be concluded that an experimental set-up of two TCPMs has given conclusive results on the preference of the electrical configuration.

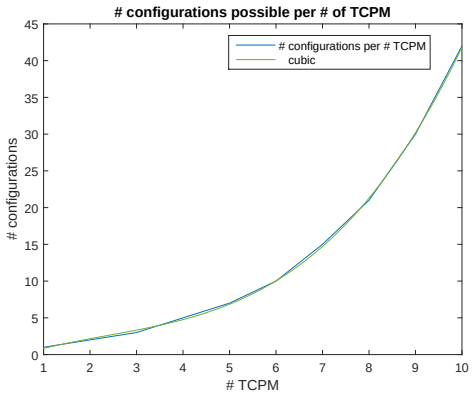

Figure 25: This graph shows the number of electrical configurations with respect to the number of elements (read TCPMs).

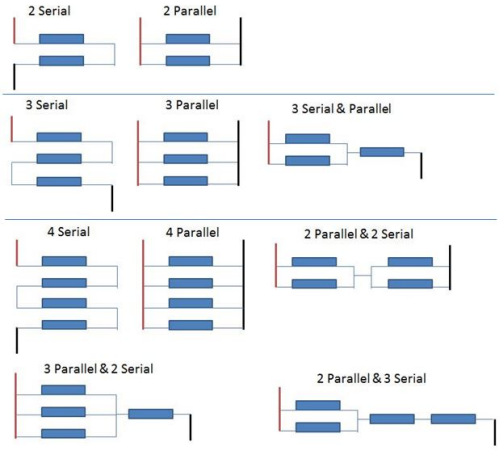

Figure 26: This visualization shows the electrical configurations for 2, 3 and 4 elements.

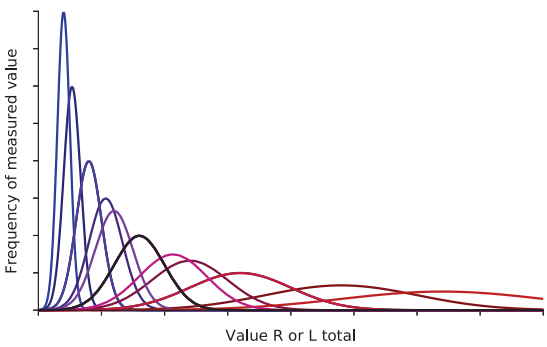

Figure 27: Colour indicates the series to parallel ratio, where blue is parallel and red is series. Black is the variance modelled for 1:1 ratio.

G. Direct versus indirect self-sensing

For this experiment two TCPMs were tested at 80 °C with the self-sensing protocol (for details see all previous appendixes) for materials and methods see report Section III. After the two TCPMs were tested as singles, they were put in a mechanical parallel structure, their centre axis 10 mm apart and the coils 1-2 mm distance, see Figure 29. They were tested in a series and parallel electrical configuration. From these experiments R suffer from a large experimental artefact and is therefore excluded from analysis. Therefore only L can be used as mapping input and only L to Δx mapping is performed. This experiment is repeated for 70 and 60 °C, which show similar results.
In Figure 30 direct mapping of two single TCPMs and the two TCPMS in a mechanical parallel structure (for series and parallel electrical configuration) is shown on the top four graphs. The lower two graphs represent results of indirect mapping (L to Δx) for series and parallel. It is clear that the series configuration performs better than the parallel configuration and that direct mapping performs better than indirect mapping. The mapping functions used for indirect mapping are purely based on equations (8)(10) and the parametric mapping formula (5), therefore neighbouring effects such as mutual inductance are not taken into account.
Mutual inductance can be calculated by equation (19) in this equation κ is the coupling factor and L_1 and L_2 are the inductances of the two TCPMS. The mutual inductance affect the total inductance depending on the direction of the electro-magnetic

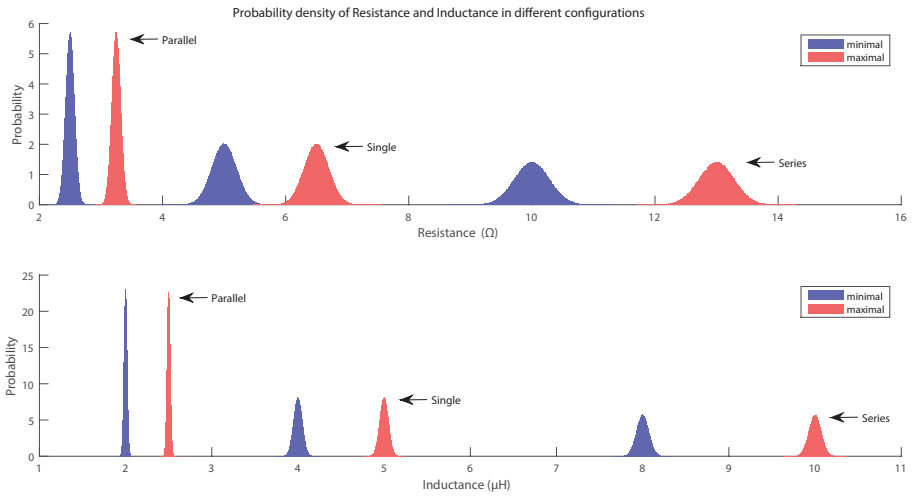

Figure 28: Colour indicates low and high values that could occur during self-sensing, where red is high and blue is low. Three different configurations are represented, from left to right: parallel, single and series. Where parallel and series are representing two TCPMs. The top graph shows the resistance - and the lower graph inductance probability density graphs. The variance is a measure of the width of each bell curve, the responsivity is the difference in value between high and low (on the x-axis).

fields of the two coils. In this experimental set-up the electro-magnetic fields are opposite, therefore the effect of the mutual inductance is negative. The total inductance of the series configuration is calculated by (17) and that of the parallel configuration is calculated by (18). In these equations L_{ts} stands for the total inductance of the series configuration and L_{tp} stands for the total inductance of the parallel configuration. L_1 and L_2 are the inductances of the two TCPMs and M is the mutual inductance.

Figure 31 shows the measured inductance of the structure and the estimated inductance for two situations. In the two top graphs $\kappa = 0$, an over-estimation is visible, since the negative mutual inductance is not taken into account. In the two bottom graphs mutual inductance is taken into account (κ is calculated for series and parallel) and the estimation is improved.

It is of great importance for the accuracy of indirect self-sensing, that the self-sensing model explicit includes mutual inductance. Where in direct self-sensing this effect is implicit, in the models parameters.

$$L_{\mathrm{ts}} = L_1 + L_2 - 2M \tag{17}$$

$$L_{\mathrm{tp}} = \frac{\frac{L_1+L_2}{2} - M^2}{L_1 L_2 + 2M} \tag{18}$$

$$M = \kappa\sqrt{L_1 L_2} \tag{19}$$

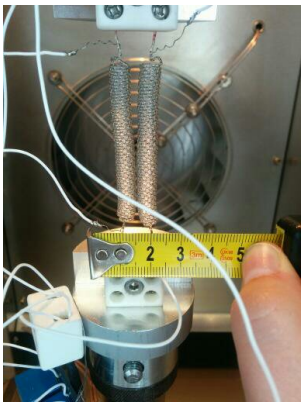

Figure 29: This photo shows the distance between two TCPMs during testing in the mechanical parallel structure.

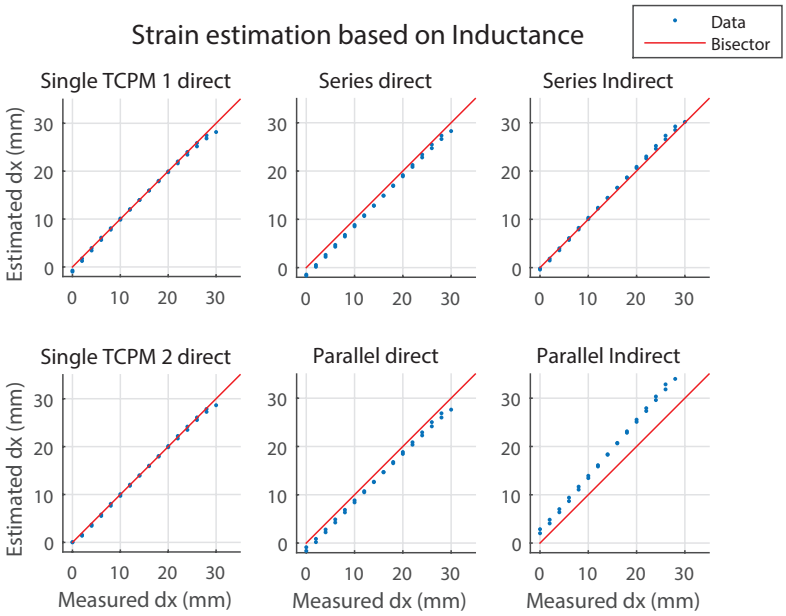

Figure 30: This figure shows top to bottom, left to right: single TCPM number 1 direct mapping, single TCPM number 2 direct mapping, structure of two TCPMs series direct mapping, structure of two TCPMS parallel direct mapping, structure of two TCPMs series indirect mapping, structure of two TCPMs parallel indirect mapping. The indirect mapping is based on single TCPM direct mapping parameters.

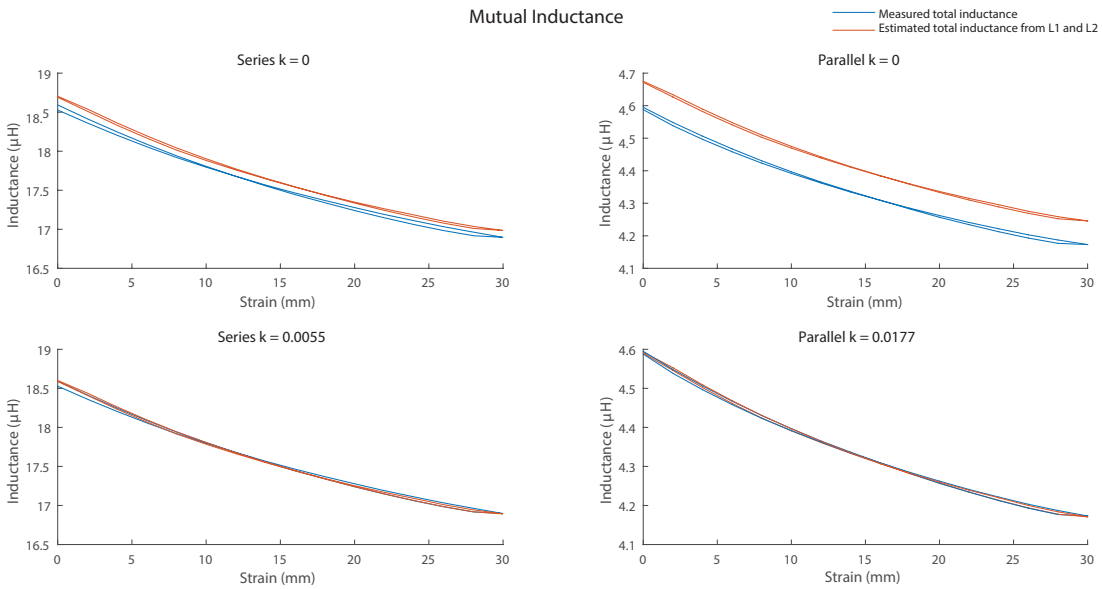

Figure 31: This figure shows left to right, top to bottom: total inductance of series and parallel configuration no mutual inductance included, series and parallel configuration mutual inductance included. Where the estimate is based on equations (8),(10) and (19). The coupling factor κ is given in the name of the plot.

References

[1] Seyed M. Mirvakili et al. "Niobium Nanowire Yarns and their Application as Artificial Muscles". In: *Advanced Functional Materials* 23.35 (Sept. 2013), pp. 4311–4316. ISSN: 1616301X.

[2] Antonello Cherubini et al. "Experimental characterization of thermally-activated artificial muscles based on coiled nylon fishing lines". In: *AIP Advances* 5.6 (June 2015), p. 067158. ISSN: 2158-3226.

[3] Carter S. Haines et al. "Artificial muscles from fishing line and sewing thread". In: *Science* 343.6173 (2014), pp. 868–872. ISSN: 1095-9203.

[4] Lianjun Wu et al. "Nylon-muscle-actuated robotic finger". In: *SPIE Smart Structures and Materials + Nondestructive Evaluation and Health Monitoring*. Ed. by Wei-Hsin Liao. Vol. 9431. Dallas, Apr. 2015, p. 94310I. ISBN: 0277-786X.

[5] Soodabeh Sharafi and Guoqiang Li. "A multiscale approach for modeling actuation response of polymeric artificial muscles". In: *Soft Matter* 11.19 (2015), pp. 3833–3843. ISSN: 1744-683X.

[6] Soheil Kianzad et al. "Nylon coil actuator operating temperature range and stiffness". In: *SPIE*. Ed. by Yoseph Bar-Cohen. Vancouver: International Society for Optics and Photonics, Apr. 2015, pp. 94301X–6.

[7] C. L. Choy, F. C. Chen, and K. Young. "Negative thermal expansion in oriented crystalline polymers". In: *Journal of Polymer Science: Polymer Physics Edition* 19.2 (Feb. 1981), pp. 335–352. ISSN: 00981273.

[8] T. Shibukawa et al. "Temperature Dependence of Shear Modulus and Density of Nylon-6". In: *Textile Research Journal* 32.12 (Dec. 1962), pp. 1011–1012. ISSN: 0040-5175.

[9] Soheil Kianzad et al. "Variable stiffness structure using nylon actuators arranged in a pennate muscle configuration". In: *SPIE*. Ed. by Yoseph Bar-Cohen. Vancouver: International Society for Optics and Photonics, Apr. 2015, 94301Z. ISBN: 0277-786X 978-1-62841-533-9.

[10] Michael C. Yip and Gunter Niemeyer. "High-performance robotic muscles from conductive nylon sewing thread". In: *2015 IEEE International Conference on Robotics and Automation (ICRA)*. IEEE, May 2015, pp. 2313–2318. ISBN: 978-1-4799-6923-4.

[11] Joost van der Weijde et al. "Self-Sensing of Deflection, Force, and Temperature for Joule-Heated Twisted and Coiled Polymer Muscles via Electrical Impedance". In: *IEEE/ASME Transactions on Mechatronics* 22.3 (June 2017), pp. 1268–1275. ISSN: 1083-4435.

[12] Joost van der Weijde et al. "Force sensing for compliant actuators using coil spring inductance". In: *2015 IEEE/RSJ International Conference on Intelligent Robots and Systems (IROS)*. Vol. 2015-Decem. IEEE, Sept. 2015, pp. 2692–2697. ISBN: 978-1-4799-9994-1.

[13] Hongjip Kim et al. "Sensorless displacement estimation of a shape memory alloy coil spring actuator using inductance". In: *Smart Materials and Structures* 22.2 (Feb. 2013), p. 025001. ISSN: 0964-1726.

[14] Toribio F. Otero and Jose G. Martinez. "Physical and chemical awareness from sensing polymeric artificial muscles. Experiments and modeling". In: *Progress in Polymer Science* 44 (May 2015), pp. 62–78. ISSN: 00796700.

[15] Andres Punning, Maarja Kruusmaa, and Alvo Aabloo. "A self-sensing ion conducting polymer metal composite (IPMC) actuator". In: *Sensors and Actuators A: Physical* 136.2 (May 2007), pp. 656–664. ISSN: 09244247.

[16] K. Ikuta, M. Tsukamoto, and S. Hirose. "Shape memory alloy servo actuator system with electric resistance feedback and application for active endoscope". In: *Proceedings. 1988 IEEE International Conference on Robotics and Automation*. IEEE Comput. Soc. Press, 1988, pp. 427–430. ISBN: 0-8186-0852-8.

[17] Takeshi Arakawa et al. "Position control of fishing line artificial muscles (coiled polymer actuators) from nylon thread". In: *Proc. SPIE 9798, Electroactive Polymer*

Actuators and Devices (EAPAD) 2016. Ed. by Yoseph Bar-Cohen and Frédéric Vidal. Vol. 9798. 882. Osaka, Apr. 2016, 97982W. ISBN: 8152789275.

[18] Ankit Tomar and Yonas Tadesse. "Multi-layer robot skin with embedded sensors and muscles". In: *SPIE*. Ed. by Yoseph Bar-Cohen and Frédéric Vidal. Dallas: International Society for Optics and Photonics, Apr. 2016, pp. 979809–12. ISBN: 9781510600393.

[19] Giacomo Moretti et al. "Experimental characterization of a new class of polymeric-wire coiled transducers." In: *SPIE Smart Structures and Materials + Nondestructive Evaluation and Health Monitoring*. Ed. by Nakhiah C. Goulbourne. Vol. 9432. Apr. 2015, 94320P. ISBN: 9781628415353.

[20] Aleksandr N. Semochkin. "A device for producing artificial muscles from nylon fishing line with a heater wire". In: *2016 IEEE International Symposium on Assembly and Manufacturing (ISAM)*. IEEE, Aug. 2016, pp. 26–30. ISBN: 978-1-5090-2412-4.

[21] Shazed Aziz et al. "Characterisation of torsional actuation in highly twisted yarns and fibres". In: *Polymer Testing* 46.46 (Sept. 2015), pp. 88–97. ISSN: 01429418.

[22] Yonas Tadesse, Lianjun Wu, and Lokesh K Saharan. "Musculoskeletal System of Bio-Inspired Robotic Systems". In: *Mechanical Engineering* 138.3 (2016), S11.

[23] Seyed M. Mirvakili et al. "Simple and strong: twisted silver painted nylon artificial muscle actuated by Joule heating". In: *SPIE*. Ed. by Yoseph Bar-Cohen. Vol. 9056. Vancouver: International Society for Optics and Photonics, Mar. 2014, p. 90560I. ISBN: 9780819499820.